

# Genuine topological Anderson insulator from impurity induced chirality reversal

Avedis Neehus,<sup>1,2</sup> Frank Pollmann,<sup>1,2</sup> and Johannes Knolle<sup>1,2,3</sup>

<sup>1</sup>Technical University of Munich, TUM School of Natural Sciences, Physics Department, 85748 Garching, Germany

<sup>2</sup>Munich Center for Quantum Science and Technology (MCQST), Schellingstr. 4, 80799 München, Germany

<sup>3</sup>Blackett Laboratory, Imperial College London, London SW7 2AZ, United Kingdom

(Dated: June 2, 2025)

We investigate a model of Dirac fermions with mass impurities which open a global topological gap even in the dilute limit. Surprisingly, we find that the chirality of this mass term, i.e., the sign of the Chern number, can be reversed by tuning the magnitude of the single-impurity scattering. Consequently, the disorder induces a phase disconnected from the simple clean limit of the topological insulator, which is achieved via an impurity resonance inducing additional bands with Chern number two. Thus, we call this impurity induced phase a genuine topological Anderson insulator. In seeming contradiction to the expectation that mass disorder is an irrelevant perturbation to the Dirac semi-metal, the tri-critical point separating these two Chern insulating phases and a thermal metal phase is located at zero impurity density and connected to the appearance of a zero energy bound state in the continuum that corresponds to a perfectly resonant mass impurity. Our conclusions based on the T-matrix expansion are substantiated by large scale Chebyshev-Polynomial-Green-Function numerics. We discuss possible experimental platforms.

*Introduction.*—Topological phases of matter [1] are not merely robust to disorder, but rather disorder is an integral part of them. This relationship is prominently exhibited in experiments on the quantum Hall effect (QHE) [2, 3] where the hallmark signature of the QHE, the resistivity plateaus, may only be observed in a dirty sample where disorder broadens the Landau levels and allows for a continuous dependence of the Fermi-level on the magnetic field [4]. Furthermore, the edge-modes corresponding to these plateaus [5] are themselves defined through their lack of back-scattering with impurities.

Nevertheless, disorder is usually seen as inimical to topological phases because it tends to localize the extended states that support them [6]. With the discovery of the topological Anderson insulator (TAI) [7–9], it appeared that there was a topological phase existing not in spite but because of disorder. Soon after, however, it was found that the disorder merely enlarges the topologically non-trivial parameter space of the clean model, in other words the disorder can be turned off continuously [10, 11].

Another phenomenon where disorder tends to delocalize rather than localize is that of Anderson anti-localization; in certain symmetry classes [12] the quantum corrections to the Drude model can drive the system into a disorder induced *metallic* phase [13], e.g. systems in symmetry class  $D$  with only particle-hole symmetry (PH) [14]. Here the metallic phase described by a *perfect metal* fixed point is called a thermal metal (TM) alluding to the fact that in the commonly discussed realizations, e.g.  $p$ -wave superconductors,  $\nu = 5/2$  fractional QH states [15–17] or Kitaev quantum spin liquids (QSL) [18, 19], the quasi-particles carry only heat currents as particle number conservation and spin-rotation invariance are broken. Because in 2D (anti-)localization corrections are marginal, numerical studies of Anderson transitions are notoriously complicated. Indeed, the body

of works [20–33] relying on network models remains inconclusive as to the structure of the RG-flow in class  $D$  systems, the main point of content being the nature and position of the tri-critical point that separates (Chern) insulators and the thermal metal phase. What is generically agreed upon is that the free fixed point controlling the clean integer QH transition is stable to weak mass disorder and the tri-critical point must be located at a finite disorder strength.

In this work we study a disorder potential  $V$ , which takes the form of a topological mass impurity, and uncover hitherto unexplored aspects of the interplay between disorder and topology: Firstly, we find a transition between different CI phases mediated by impurity resonances whose hybridization with the Dirac cone leads to the emergence of *new topological mobility gaps* that have no clean equivalent [37]. We dub this phase that is enabled by a Chernful impurity resonance band a genuine TAI (GTAI). Secondly, we show that our model realizes the tri-critical point of class  $D$  systems at *zero impurity density*, i.e., the clean Dirac fermions seem unstable to mass disorder, see Fig. 1 (a). For weak scatterers we observe that  $V$  opens a gap with Chern number  $C = 1$  at *any* finite density. Since the Haldane model is recovered in the limit of the impurity density going to one, this does not represent the GTAI. While the Haldane model itself is stable against weak perturbations, we find that for strong enough  $V$  there is a region of densities which hosts a thermal metal phase. However, for strong dilute impurities there appears yet again a Chern insulating phase, which is a GTAI with the effective chirality of the impurity potential *reversed* such that  $C = -1$ , see Fig. 1 (c). At the tri-critical point between the two Chern phases and the TM we find a zero energy bound state (ZBS) which we could not associate with known mechanisms [34, 36]. Strikingly, the ZBS corresponds to

an impurity whose renormalized potential is a divergent Dirac *mass* term. We discuss these results both within the T-matrix approximation and state-of-the-art exact numerics with up to  $O(10^9)$  sites.

*The model.*— We consider a nearest neighbour (NN) tight-binding model of spin polarized fermions  $c$  on a hexagonal lattice together with an impurity potential that takes the form of the imaginary next-NN hopping, Fig. 1 (b):

$$H(t_2, \rho) = -t \sum_{\langle i,j \rangle} c_i^\dagger c_j + \sum_{\bigcirc} p(\bigcirc, \rho) V_{\bigcirc}(t_2) \quad (1)$$

$$V_{\bigcirc} = t_2 \sum_{\langle\langle i,j \rangle\rangle \in \bigcirc} e^{i\Phi_{i,j}} c_i^\dagger c_j. \quad (2)$$

It is distinguished from the regular Haldane model [35] by introduction of the random binary variable  $p$  which is equal to 1 on a fraction  $\rho$  of all the available honeycombs and 0 otherwise. We let  $t_2 > 0$  and take  $|\Phi| = \frac{\pi}{2}$  to study the rich phase diagram of class  $D$  systems and keep the impurity potential simple [44]. However, the existence of the GTAI is generic for a finite range of  $\Phi$ .

*T-matrix Approximation.*— First we study the system perturbatively and introduce  $T$  as the renormalized potential  $V$  taking into account multiple scattering events off of a single impurity. It is computed by [38]

$$T_{\bigcirc}(E) = (1 - V_{\bigcirc} G_0(E))^{-1} V_{\bigcirc}, \quad (3)$$

where  $G_0(E)$  is the lattice Greens function of the clean system. Like the potential  $V$ ,  $T$  is represented by a  $6 \times 6$  matrix which we calculate exactly. Following Ostrovsky *et al.* [39–41] we project  $T$  into the basis of the two-flavor Dirac spinors in terms of which we may write the low-energy theory  $H_{\mathbf{R}} = \int d\mathbf{r} \psi^\dagger(\mathbf{r}) h_{\mathbf{R}}(\mathbf{r}) \psi(\mathbf{r})$  of the model with an impurity at a *certain* position  $\mathbf{R}$  as

$$h_{\mathbf{R}}(\mathbf{r}) = \frac{3t}{2} (\tau_z \sigma_x i \partial_x + \sigma_y i \partial_y) + \delta_{\mathbf{a}}(\mathbf{r} - \mathbf{R}) \frac{3t_2}{2} (-\tau_x \sigma_z i \partial_x + \tau_y i \partial_y + \sigma_z \tau_z). \quad (4)$$

Here the Paulis  $\sigma$  act on the sublattice and  $\tau$  on the valley degree of freedom of the Dirac spinors  $\psi$  and we have emphasized ‘certain’ because there is a position dependent rotation of the the valley spin around  $\tau_z$ . Note that the gradient contribution of the impurity is related to the clean Dirac hamiltonian via inversion and the exchange of  $\tau$  and  $\sigma$ , and therefore can be thought of as a locally chirality reversing effect. However, as for short range scatterers the last constant contribution is dominant the effect should be negligible. Indeed, the crucial point is that the gradient terms generate a second contribution in the s-wave channel of the T-matrix:

$$T_{\mathbf{R}}(0) = \frac{A3\sqrt{3}t_2}{t_2^2/t_c^2 - 1} [\sigma_z \tau_z + \frac{t_2}{t_c} \sigma_x (\tau_x \cos f_{\mathbf{R}} + \tau_y \sin f_{\mathbf{R}})]$$

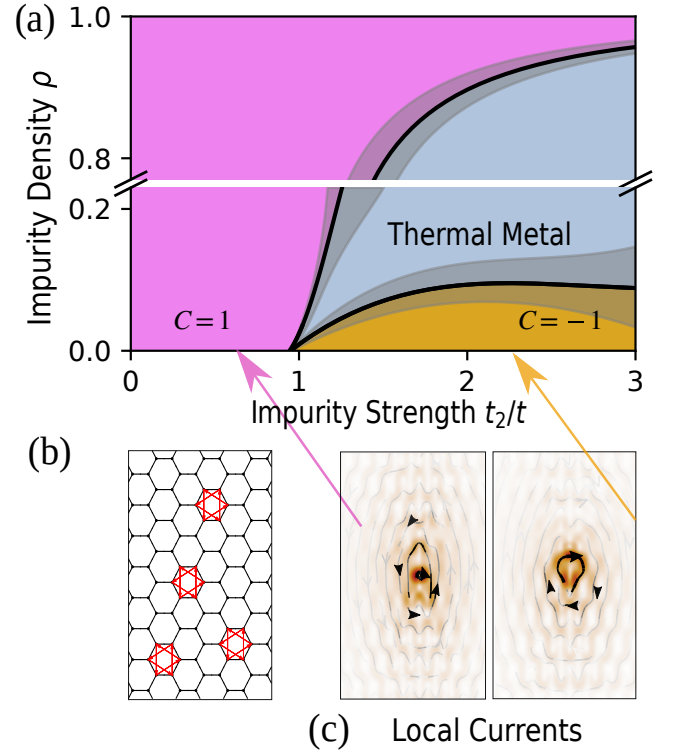


FIG. 1. (a) Phase diagram of the nearest-neighbour honeycomb model with topological mass disorder, which is depicted in panel (b). The red arrows represent the imaginary potential. (c) Streamplot of the local current vector field around a single impurity. The orange hue is proportional to the magnitude of the local vector field. The probability currents are evaluated on a state with energy close to 0, inside the  $C = 1$  (left) and the  $C = -1$  phase (right).

where  $f_{\mathbf{R}} = 2\mathbf{K} \cdot \mathbf{R}$ , with  $\mathbf{K}$  being the usual Dirac point, takes values in multiples of  $\frac{2\pi}{3}$ ,  $t_c = \frac{2\sqrt{3}\pi}{3\sqrt{3}+2\pi}t \approx t$  and  $A$  is the unit cell area. Here we have made explicit the position dependent rotation of the valley spin first pointed out by Schelter *et al.* [41]. To first order in the impurity density, the self-energy of the configuration averaged Green’s function is given by the configuration averaged T-matrix. Therefore, the valley off-diagonal terms cancel and at zero energy we obtain, without self-consistency,

$$\Sigma(0) = \frac{\rho}{A} \langle T_{\bigcirc}(0) \rangle = \frac{\rho 3\sqrt{3}t_2}{t_2^2/t_c^2 - 1} \sigma_z \tau_z. \quad (5)$$

Remarkably, expression Eq. (5) accounts for all of the peculiar features of the phase diagram. First, we observe that for small  $t_2$  the gap is linear in both  $\rho$  and  $t_2$ . In particular *any* finite density of these impurities is enough to open a topological gap with  $C = \text{sgn } t_2$ . This is natural consequence of the critical system having single particle correlation that decay with the inverse of the distance. Second, beyond the critical value  $t_c$  the sign of the mass term switches and therefore so does the Chern number.

Third, at  $t_c$  the T-matrix has a pole. This signals the appearance of two degenerate zero energy bound states (ZBS) [45] acting as a seed for the thermal metal. While the TM phase is beyond the T-matrix description, it is still clear that a dilute number of ZBS alone can not be responsible for a metallic phase, unless the spectral gap of the Dirac fermions is closed. Extending the calculation to energies away from the PH-symmetric point we obtain a closed analytical but lengthy expression which we show in the supplemental material (SM). At  $t_2$  close but not equal to  $t_c$  we get for energies  $t \gg E \gg |t_2 - t_c|$  [51]:

$$\Sigma(E) \approx \frac{\rho}{A} \left( \gamma^{-1} \sigma_0 \tau_0 + \frac{A3\sqrt{3}t_2}{t_2^2/t_c^2 - 1} \gamma^{-2} \sigma_z \tau_z \right) \quad (6)$$

$$\text{with } \gamma = \lim_{r \rightarrow 0} G_0(E, r) - G_0(0, r) \approx \frac{1}{2\pi v^2} E \log iE. \quad (7)$$

We observe that  $\Sigma_{00}$  is divergent, however at the value of the discontinuity, i.e.,  $E = 0$ ,  $\Sigma_{00}$  is pinned to 0 by PH-symmetry. Therefore we can conclude that the spectral gap is indeed closed by an impurity resonance, the role of which will be clarified in the discussion following the numerical results.

*Numerical Results.*— The Chebychev polynomial Green's function (CPGF) expansion is a formally exact rewriting of the Green's function of the rescaled Hamiltonian  $h$  whose spectrum lies in the interval  $[-1, 1]$ :

$$G(E + i\eta) = \sum_{n=0}^{\infty} \lambda_n(E, \eta) P_n(h),$$

where  $\lambda_n$  are system independent coefficients and  $T_n$  is the  $n$ th order Chebyshev polynomial. Physical observables like the spectral function  $A(E, k) = -1/\pi \Im \text{Tr} G^r(E, k)$  or the Kubo-Bastin conductivities [50]

$$\sigma_{ij} = \frac{\hbar}{2\pi} \int d\epsilon \text{Tr} (J_i \partial_\epsilon G^r J_j - J_j \partial_\epsilon G^a J_i) (G^a - G^r)$$

are expressed as traces of retarded  $G^r$  ( $\eta = i0^+$ ) and advanced  $G^a$  ( $\eta = i0^-$ ) Greens functions and computationally easy operators like the charge currents  $J$ . The sum of  $T_n$  applied to a vector can be computed very efficiently using the Chebyshev recursion relations. Because of the sparseness of  $P_n(h)$  [60] the trace over the whole Hilbert-space can be reduced to just one random vector with an error of  $O(N^{-\frac{1}{2}})$  [52],  $N$  being the total number of orbitals. Combining this with a cutoff for  $n$  proportional to  $\eta^{-1}$  we are able to carry out large scale simulations (up to  $N = O(10^9)$ ,  $\eta = O(10^{-4})$ ) using the *KITE* software package [53] to calculate the density of states (DOS) and longitudinal conductivities  $\sigma_{xx}$ . While the calculation of  $\sigma_{xx}$  can be simplified to require only one expansion [54], calculations of the Hall conductivity  $\sigma_{xy}$  require a double Chebyshev expansion. Nevertheless, we are able to access reasonably large system

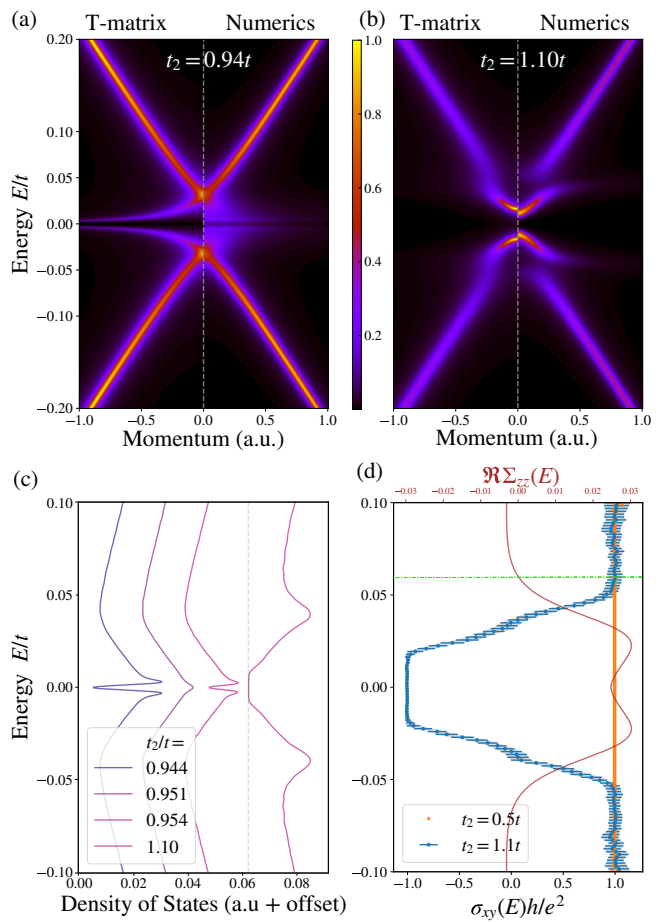


FIG. 2. (a) / (b) Spectral function along a momentum path through the Dirac point for  $\rho = 0.15\%$  and  $t_2 = 0.94/1.10$  rescaled to a maximum value of 1. The left half of each panel is computed analytically within the T-matrix approximation. (c) Density of states calculated using the CPGF for various values of  $t_2$ . For better visibility the values have been off-set by a constant which is zero for the smallest  $t_2$  and increased by 0.017 (a.u.) for every increasing value of  $t_2$ . The vertical green dashed lines shows the origin of the rightmost curve. (d) Hall conductivity and it's standard deviation computed using the CPGF expansion averaged over 64 disorder configurations. We also plot the real part of the self-energy mass  $\Sigma_{zz}$  at  $t_2 = 1.1$  whose values are indicated by the top scale. For reference, we also include the Hall conductivity data at  $t_2 = 0.5$ . The horizontal dashed line indicates the zero crossing of  $\Re \Sigma_{zz}$ .

sizes ( $N = O(10^7)$ ,  $\eta = O(10^{-3})$ ) using the Fast Fourier-Chebyshev approach [55].

We estimated the phase boundaries in Fig.1 (a) by computing the periodic boundary version of the localization tensor [56], and the Bott-index [57] for system sizes  $N = O(10^3)$  and 40 disorder averages. The thermal metal phase can be identified by a diverging localization tensor and a non-quantized small value of the disorder-averaged Bott-index. We also calculated the Chern number for a point in the  $C = -1$  phase using Fukui's method [58] on the Brillouin-Torus of a

super-cell. The obtained phase boundaries were verified using CPGF simulations for some exemplary points by scaling of the conductivity  $\sigma_{xx}$  and a transition to logarithmically divergent DOS on the TM side [59], further information can be found in the SM. We note that the transition to the thermal metal phase can not simply be determined by the onset of a diverging DOS at zero energy, as we observe that the insulating state may have a non-logarithmically divergent DOS. This divergence is consistent with the prediction of a Griffiths phase in symmetry class D where it appears as a result of rare impurity configurations with a large separation [26]. The proposed mechanism is that zero modes bound to these impurities contribute to the DOS at a hybridization gap exponentially small in the separation. The existence of a Griffiths phase in our model hence suggests that ZBS exist also at densities beyond the T-matrix description, where, however, they do not correspond to a diverging topological mass term.

*Chirality reversal at the tri-critical point.*— Focusing now on  $\rho \ll 1$  and  $t_2 \approx 1$  we observe that we can identify  $t_c$  by the coalescing of the particle and hole resonance at zero energy, Fig. 2 (c). Furthermore, at finite  $\rho$  the TM phase extends over a finite region of the parameter space (not visible for parameters of the plot). The value at which the resonances meet is shifted slightly towards larger  $t_2$  with increasing  $\rho$  due to self-consistency effects on  $t_c(\Sigma(E))$ . For example at  $\rho = 0.15\%$  it's around 0.950, while it is 0.955 for  $\rho = 0.5\%$ . The spectral function close to  $t_2 = t_c$  reveals an additional structure emanating from the tip of the gapped Dirac cone, Fig. 2 (a). Within the T-matrix approximation this seems like a sharp mode becoming asymptotically flat while approaching the value of the effective spectral gap. On top of self-consistency effects, higher order impurity scattering effects change the picture slightly by broadening this band, however, scaling of the DOS with  $\eta$  suggest that the spectral gap is maintained even including these processes, as further discussed in the SM. With increasing  $t_2$  this almost flat band eventually detaches from the Dirac cone creating a second mobility gap with  $C = 1$  then curving further upward until the  $C = 1$  gap is closed. Figure 2 (b) shows the spectral function for such an intermediary value with a  $C = 1$  gap at finite energy. Remarkably, this  $C = 1$  gap implies that the resonance-hybridized band carries a Chern number of  $\pm 2$ ; We emphasize that due to the emergence of the additional mobility gaps there is no corresponding clean Haldane model that reproduces the whole topological information as the unit cell must have a minimum of 4 sites [74]. This highlights the essential role played by the impurity resonance which could not appear in a clean system justifying the use of the term genuine.

We note that here we have the interesting situation that the sign of the effective mass term changes within

the spectrum and thus the argument relating the topological mass of the Dirac fermions to the Hall conductivity, which is a Fermi-sea property, may be invalid. The problem of evaluating the topology of a system with energy dependent self-energy has been discussed in the context of the many-body Chern number [61, 62], and the result, that the topology only depends on the renormalized Green function at chemical potential, is also applicable to our case. We give an independent confirmation of this by computing  $\sigma_{xy}$  using the CPGF expansion, Fig. 2 (d).

*Discussion and Outlook.*— While the thermal quantum Hall transition lies at zero mean mass  $\mu = 0$  and zero mass variance  $\sigma^2 = 0$  with  $\sigma^2$  being marginally irrelevant [46, 47], recent results [30, 32, 33] from field theory and numerics agree that the tri-critical point, with a transition to a thermal metal, is located at  $\mu = 0$  but a finite  $\sigma^2$ . To reconcile this with the fact that the variance  $\sigma^2 \propto \rho(1 - \rho)t_2^2$  of our impurity distribution is zero at zero density, we note that this apparent inconsistency may be resolved by estimating the mass variance from the renormalized impurity potential  $T$  whose divergence at the tri-critical point can make  $\sigma^2$  finite when taking the limit  $\rho \rightarrow 0$ . Another possible explanation is that in addition to mass disorder the impurities act as vortex disorder, via the introduction of effective  $\pi$ -fluxes, which can be large independently of  $\rho$ . Indeed this possibility has led Read and Green to conjecture that the thermal Hall transition is generically unstable to the thermal metal [16]. However, as demonstrated in the SM, we were not able to identify such a vortex defect using the paradigm for the classification of defect Hamiltonians [36].

The formation of a ZBS in the continuum as a result of a parametric tuning of two resonances is reminiscent of the Friedrich-Wintgen mechanism [48]. However, given that both resonances become infinitely sharp, we posit that it is a distinct phenomenon; namely, that the particle-hole symmetry related Chern critical impurity resonances interfere destructively as they cross at  $E = 0$ , thereby forming two bound states of opposite chirality. A picture thus emerges where the continuum of extended states hosting the BIC is itself created by the impurity.

To summarize, we have introduced an example of a GTAI, where impurity resonances change the topology of the clean limit and may even introduce additional topological mobility gaps. Remarkably, these resonance-hybridized Chernful bands correspond to quasiparticles that have finite momentum support. Furthermore, our model shows that Anderson tri-critical point of class D may arise at zero impurity density through a resonant impurity potential which can bind fermionic zero modes.

We note that the necessary cancelling of the inter-valley contributions via the position dependent valley spin rotation is also possible for certain periodic arrangements of impurities and the GTAI, like the TAI, is *not*

necessarily an Anderson insulator in the sense that it does not depend on localization effects [75]. Therefore, the GTAI could also be observed for certain superlattice potentials.

We believe that our model is relevant to a variety of physical systems, ranging from topological bosons, e.g. in photonics and magnonics, to the amorphous Kitaev model. In photonics, for example, the Haldane model can be realized using gyromagnetic scattering centers to open a topological gap, and individual control of the local magnetic field has already been demonstrated [63–65]. Similar control can also be achieved in other proposals, both photonic and electronic, where the topological mass term can be realized through scattering centers in artificial graphene [66–68]. In magnonics our model could be realized by impurities, e.g. chiral adsorbed molecules [69], inducing a density of local Dzyaloshinskii–Moriya interactions in honeycomb ferromagnets. We would also like to point out that the impurity potential studied in this work has formal similarity with the problem of adatom absorption in graphene leading to Kane-Mele mass impurities [70, 71]. While in the Kane-Mele version one can not observe a GTAI, our analysis provides two important insights that should still apply. Firstly, a leading order expansion of the impurity potential around the Dirac points [72] is not sufficient to get accurate estimates of the gap for strong impurities. Second, we find a natural explanation for the cancelling of inter-valley scattering effects via random absorption [73] and can even predict periodic configurations where inter-valley scattering is suppressed.

Our study is also linked to recent works on the amorphous Kitaev model where the presence of odd-plaquettes opens a topological gap towards a Chiral QSL [76, 77]. Taking into account that the effective three-spin term generated by a magnetic field may also be obtained perturbatively by integrating out the triangles of the Yao-Kivelson model [78, 79], we argue that for moderate amounts of amorphous disorder, the odd-plaquettes can be considered as generating a local (Majorana) topological mass term of the type considered here, which is consistent with the observed linear dependence between the gap and the odd-plaquette density [77].

The mechanism of ‘local TR-breaking’ impurities opening a global topological gap may also be relevant to the emerging field of chiral imprinting by adsorption of chiral molecules [80–82] and the stability of the Dirac cones at the surface of topological insulators or superconductors to, e.g., magnetic impurities [83, 84]. Beyond the realization in concrete systems, we hope this work will also inspire future studies into Anderson criticality in class  $D$ , as well as this new type of ZBS. Furthermore, our method of creating a topological gap may also prove useful to further exploration of the criticality of Dirac fermions in symmetry class  $A$  [85], because the small coordination number allows for very efficient CPGF calcu-

lations which rely on the sparseness of  $P_n$ .

*Acknowledgements*— We thank Santiago Gimenez de Castro for providing us with his implementation of the FastCheb algorithm and Aires Ferreira, João Manuel Viana Parente Lopes, and Simão Meneses João for providing support with QuantumKite. Furthermore, we acknowledge helpful discussions with Jonas Habel, Alaric Sanders, Wojciech Jankowski and Rao Peng. We also thank Aires Ferreira for providing thoughtful feedback and pointing us to the literature of adatom absorption in graphene.

We acknowledge support from the Imperial-TUM flagship partnership, the Deutsche Forschungsgemeinschaft (DFG, German Research Foundation) under Germany’s Excellence Strategy–EXC–2111–390814868, DFG grants No. KN1254/1-2, KN1254/2-1, and TRR 360 - 492547816 and from the International Centre for Theoretical Sciences (ICTS) for the program "Frustrated Metals and Insulators" (code: ICTS/frumi2022/9), as well as the Munich Quantum Valley, which is supported by the Bavarian state government with funds from the Hightech Agenda Bayern Plus. F. P. acknowledges support from European Union’s Horizon 2020 research and innovation program under grant agreement No. 771537.

- 
- [1] R. Moessner and J. E. Moore, *Topological Phases of Matter* (Cambridge University Press, 2021).
  - [2] K. von Klitzing, The quantized Hall effect, *Rev. Mod. Phys.* **58**, 519 (1986).
  - [3] K. V. Klitzing, G. Dorda, and M. Pepper, New method for high-accuracy determination of the fine-structure constant based on quantized hall resistance, *Phys. Rev. Lett.* **45**, 494 (1980).
  - [4] J. Bellissard, A. van Elst, and H. Schulz-Baldes, The Non-Commutative Geometry of the Quantum Hall Effect, *Journal of Mathematical Physics* **35**, 5373 (1994), arXiv:9411052v1 [cond-mat].
  - [5] J.-W. Rhim, J. H. Bardarson, and R.-J. Slager, Unified bulk-boundary correspondence for band insulators, *Phys. Rev. B* **97**, 115143 (2018).
  - [6] P. W. Anderson, Absence of diffusion in certain random lattices, *Phys. Rev.* **109**, 1492 (1958).
  - [7] J. Li, R.-L. Chu, J. K. Jain, and S.-Q. Shen, Topological anderson insulator, *Phys. Rev. Lett.* **102**, 136806 (2009).
  - [8] C. W. Groth, M. Wimmer, A. R. Akhmerov, J. Tworzydło, and C. W. J. Beenakker, Theory of the topological anderson insulator, *Physical Review Letters* **103**, 10.1103/physrevlett.103.196805 (2009).
  - [9] E. J. Meier, F. A. An, A. Dauphin, M. Maffei, P. Massignan, T. L. Hughes, and B. Gadway, Observation of the topological anderson insulator in disordered atomic wires, *Science* **362**, 929 (2018).
  - [10] E. Prodan, Three-dimensional phase diagram of disordered hgte/cdte quantum spin-hall wells, *Phys. Rev. B* **83**, 195119 (2011).
  - [11] S. Lieu, D. K. Lee, and J. Knolle, Disorder protected and induced local zero-modes in longer-range kitaev chains,

- Physical Review B **98**, 134507 (2018).
- [12] A. Altland and M. R. Zirnbauer, Nonstandard symmetry classes in mesoscopic normal-superconducting hybrid structures, *Physical Review B* **55**, 1142 (1997).
- [13] F. Evers and A. D. Mirlin, Anderson transitions, *Rev. Mod. Phys.* **80**, 1355 (2008).
- [14] M. Bocquet, D. Serban, and M. Zirnbauer, Disordered 2d quasiparticles in class d: Dirac fermions with random mass, and dirty superconductors, *Nuclear Physics B* **578**, 628 (2000).
- [15] T. Senthil and M. P. A. Fisher, Quasiparticle localization in superconductors with spin-orbit scattering, *Phys. Rev. B* **61**, 9690 (2000).
- [16] N. Read and D. Green, Paired states of fermions in two dimensions with breaking of parity and time-reversal symmetries and the fractional quantum hall effect, *Phys. Rev. B* **61**, 10267 (2000).
- [17] C. R. Laumann, A. W. Ludwig, D. A. Huse, and S. Trebst, Disorder-induced majorana metal in interacting non-abelian anyon systems, *Physical Review B - Condensed Matter and Materials Physics* **85**, 161301 (2012).
- [18] J. Nasu, J. Yoshitake, and Y. Motome, Thermal transport in the kitaev model, *Physical Review Letters* **119**, 10.1103/PhysRevLett.119.127204 (2017).
- [19] C. N. Self, J. Knolle, S. Iblisdir, and J. K. Pachos, Thermally induced metallic phase in a gapped quantum spin liquid: Monte carlo study of the kitaev model with parity projection, *Physical Review B* **99**, 045142 (2019).
- [20] S. Cho and M. P. A. Fisher, Criticality in the two-dimensional random-bond ising model, *Phys. Rev. B* **55**, 1025 (1997).
- [21] J. T. Chalker, N. Read, V. Kagalovsky, B. Horowitz, Y. Avishai, and A. W. W. Ludwig, Thermal metal in network models of a disordered two-dimensional superconductor, *Phys. Rev. B* **65**, 012506 (2001).
- [22] N. Read and A. W. W. Ludwig, Absence of a metallic phase in random-bond ising models in two dimensions: Applications to disordered superconductors and paired quantum hall states, *Phys. Rev. B* **63**, 024404 (2000).
- [23] I. A. Gruzberg, N. Read, and A. W. W. Ludwig, Random-bond ising model in two dimensions: The nishimori line and supersymmetry, *Phys. Rev. B* **63**, 104422 (2001).
- [24] F. Merz and J. T. Chalker, Two-dimensional random-bond ising model, free fermions, and the network model, *Phys. Rev. B* **65**, 054425 (2002).
- [25] F. Merz and J. T. Chalker, Negative scaling dimensions and conformal invariance at the nishimori point in the  $\pm j$  random-bond ising model, *Phys. Rev. B* **66**, 054413 (2002).
- [26] A. Mildenerger, F. Evers, R. Narayanan, A. D. Mirlin, and K. Damle, Griffiths phase in the thermal quantum hall effect, *Phys. Rev. B* **73**, 121301 (2006).
- [27] A. Mildenerger, F. Evers, A. D. Mirlin, and J. T. Chalker, Density of quasiparticle states for a two-dimensional disordered system: Metallic, insulating, and critical behavior in the class-d thermal quantum hall effect, *Phys. Rev. B* **75**, 245321 (2007).
- [28] V. Kagalovsky and D. Nemirowsky, Universal critical exponent in class d superconductors, *Phys. Rev. Lett.* **101**, 127001 (2008).
- [29] V. Kagalovsky and D. Nemirowsky, Critical fixed points in class d superconductors, *Phys. Rev. B* **81**, 033406 (2010).
- [30] M. V. Medvedeva, J. Tworzydło, and C. W. J. Beenakker, Effective mass and tricritical point for lattice fermions localized by a random mass, *Phys. Rev. B* **81**, 214203 (2010).
- [31] B. Lian, J. Wang, X.-Q. Sun, A. Vaezi, and S.-C. Zhang, Quantum phase transition of chiral majorana fermions in the presence of disorder, *Phys. Rev. B* **97**, 125408 (2018).
- [32] Z. Pan, T. Wang, T. Ohtsuki, and R. Shindou, Renormalization group analysis of dirac fermions with a random mass, *Physical Review B* **104**, 10.1103/physrevb.104.174205 (2021).
- [33] T. Wang, Z. Pan, T. Ohtsuki, I. A. Gruzberg, and R. Shindou, Multicriticality of two-dimensional class-d disordered topological superconductors, *Phys. Rev. B* **104**, 184201 (2021).
- [34] C. W. Hsu, B. Zhen, A. D. Stone, J. D. Joannopoulos, and M. Soljačić, Bound states in the continuum, *Nature Reviews Materials* **1**, 16048 (2016).
- [35] F. D. Haldane, Model for a quantum hall effect without landau levels: Condensed-matter realization of the "parity anomaly", *Phys. Rev. Lett.* **61**, 2015 (1988).
- [36] J. C. Y. Teo and C. L. Kane, Topological defects and gapless modes in insulators and superconductors, *Phys. Rev. B* **82**, 115120 (2010).
- [37] With a finite real part we would introduce an additional chemical potential.
- [38] S. Takeno, Self-energy and t-matrix in many-impurity problems in solids, *Physics Letters A* **28**, 641 (1969).
- [39] P. Kot, J. Parnell, S. Habibian, C. Straßer, P. M. Ostrovsky, and C. R. Ast, Band dispersion of graphene with structural defects, *Phys. Rev. B* **101**, 235116 (2020).
- [40] P. M. Ostrovsky, M. Titov, S. Bera, I. V. Gornyi, and A. D. Mirlin, Diffusion and criticality in undoped graphene with resonant scatterers, *Phys. Rev. Lett.* **105**, 266803 (2010).
- [41] J. Schelter, P. M. Ostrovsky, I. V. Gornyi, B. Trauzettel, and M. Titov, Color-dependent conductance of graphene with adatoms, *Phys. Rev. Lett.* **106**, 166806 (2011).
- [42] F. Pollmann and A. M. Turner, Detection of symmetry-protected topological phases in one dimension, *Phys. Rev. B* **86**, 125441 (2012).
- [43] M. McGinley and N. R. Cooper, Fragility of time-reversal symmetry protected topological phases, *Nature Physics* **16**, 1181 (2020).
- [44] Note that when taking the full expression and completing  $\gamma(0) = 0$  we do recover Eq. 5. However, the energy and the  $t_2$  limit do not coincide because the self-energy is discontinuous.
- [45] The divergence must still occur even when including self-consistency effects, although the critical value of  $t_2$  could change, however it can be cut off by effects ignored in our T-matrix description. We believe that the disorder strength will nonetheless be large enough for the thermal Hall transition to be absent. This is supported by our numerics going as low as  $\rho = 0.0015$ .
- [46] A. W. W. Ludwig, M. P. A. Fisher, R. Shankar, and G. Grinstein, Integer quantum hall transition: An alternative approach and exact results, *Phys. Rev. B* **50**, 7526 (1994).
- [47] T. Morimoto, A. Furusaki, and C. Mudry, Anderson localization and the topology of classifying spaces, *Phys. Rev. B* **91**, 235111 (2015).
- [48] H. Friedrich and D. Wintgen, Interfering resonances and bound states in the continuum, *Phys. Rev. A* **32**, 3231 (1985).

- [49] E. Grosfeld and A. Stern, Electronic transport in an array of quasiparticles in the non-abelian quantum hall state, *Phys. Rev. B* **73**, 201303 (2006).
- [50] A. Crépieux and P. Bruno, Theory of the anomalous hall effect from the kubo formula and the dirac equation, *Phys. Rev. B* **64**, 014416 (2001).
- [51] The sparseness of  $T_n(h)$  depends on  $n$  among other factors. The decreasing sparseness with higher  $n$  provides a bottleneck for the resolutions one can reach using the stochastic trace method.
- [52] A. Weiße, G. Wellein, A. Alvermann, and H. Fehske, The kernel polynomial method, *Rev. Mod. Phys.* **78**, 275 (2006).
- [53] S. M. João, M. Anđelković, L. Covaci, T. G. Rapoport, J. M. V. P. Lopes, and A. Ferreira, Kite: high-performance accurate modelling of electronic structure and response functions of large molecules, disordered crystals and heterostructures, *Royal Society Open Science* **7**, 191809 (2020).
- [54] A. Ferreira and E. R. Mucciolo, Critical delocalization of chiral zero energy modes in graphene, *Phys. Rev. Lett.* **115**, 106601 (2015).
- [55] S. G. de Castro, J. a. M. V. P. Lopes, A. Ferreira, and D. A. Bahamon, Fast fourier-chebyshev approach to real-space simulations of the kubo formula (2024).
- [56] R. Resta, Electron localization in the quantum hall regime, *Phys. Rev. Lett.* **95**, 196805 (2005).
- [57] M. B. Hastings and T. A. Loring, Topological Insulators and  $C^*$ -Algebras: Theory and Numerical Practice, *Annals of Physics* **326**, 1699 (2010), arXiv:1012.1019.
- [58] T. Fukui, Y. Hatsugai, and H. Suzuki, Chern Numbers in Discretized Brillouin Zone: Efficient Method of Computing (Spin) Hall Conductances, *Journal of the Physical Society of Japan* **74**, 1674 (2005), arXiv:0503172v2 [cond-mat].
- [59] D. A. Ivanov, The supersymmetric technique for random-matrix ensembles with zero eigenvalues, *Journal of Mathematical Physics* **43**, 126 (2002).
- [60] Note that this rare-region explanation is also restricted to small  $\rho$ , while the divergent DOS in the insulator is observed even beyond this regime.
- [61] Z. Wang and S.-C. Zhang, Simplified topological invariants for interacting insulators, *Phys. Rev. X* **2**, 031008 (2012).
- [62] L. Peralta Gavensky, S. Sachdev, and N. Goldman, Connecting the many-body chern number to luttinger's theorem through středa's formula, *Phys. Rev. Lett.* **131**, 236601 (2023).
- [63] Z. Wang, Y. Chong, J. D. Joannopoulos, and M. Soljačić, Observation of unidirectional backscattering-immune topological electromagnetic states, *Nature* **461**, 772 (2009).
- [64] P. Zhou, G.-G. Liu, Y. Yang, Y.-H. Hu, S. Ma, H. Xue, Q. Wang, L. Deng, and B. Zhang, Observation of photonic antichiral edge states, *Phys. Rev. Lett.* **125**, 263603 (2020).
- [65] G.-G. Liu, Y. Yang, X. Ren, H. Xue, X. Lin, Y.-H. Hu, H.-x. Sun, B. Peng, P. Zhou, Y. Chong, *et al.*, Topological anderson insulator in disordered photonic crystals, *Physical Review Letters* **125**, 133603 (2020).
- [66] M. Gibertini, A. Singha, V. Pellegrini, M. Polini, G. Vignale, A. Pinczuk, L. N. Pfeiffer, and K. W. West, Engineering artificial graphene in a two-dimensional electron gas, *Phys. Rev. B* **79**, 241406 (2009).
- [67] S. Lannebère and M. G. Silveirinha, Link between the photonic and electronic topological phases in artificial graphene, *Phys. Rev. B* **97**, 165128 (2018).
- [68] S. Lannebère and M. G. Silveirinha, Photonic analogues of the haldane and kane-mele models, *Nanophotonics* **8**, 1387 (2019).
- [69] R. Alhyder, A. Cappellaro, M. Lemeshko, and A. G. Volosniev, Achiral dipoles on a ferromagnet can affect its magnetization direction, *The Journal of Chemical Physics* **159** (2023).
- [70] C. Weeks, J. Hu, J. Alicea, M. Franz, and R. Wu, Engineering a robust quantum spin hall state in graphene via adatom deposition, *Phys. Rev. X* **1**, 021001 (2011).
- [71] F. J. d. Santos, D. A. Bahamon, R. B. Muniz, K. McKenna, E. V. Castro, J. Lischner, and A. Ferreira, Impact of complex adatom-induced interactions on quantum spin hall phases, *Phys. Rev. B* **98**, 081407 (2018).
- [72] M. Milletari and A. Ferreira, Quantum diagrammatic theory of the extrinsic spin hall effect in graphene, *Phys. Rev. B* **94**, 134202 (2016).
- [73] H. Jiang, Z. Qiao, H. Liu, J. Shi, and Q. Niu, Stabilizing topological phases in graphene via random adsorption, *Phys. Rev. Lett.* **109**, 116803 (2012).
- [74] Odd-plaquettes meaning that the plaquette has an odd number of edges.
- [75] Note that each individual ground state may still be adiabatically connected to one that commutes with the elementary translations of the honeycomb lattice.
- [76] G. Cassella, P. d'Ornellas, T. Hodson, W. M. H. Natori, and J. Knolle, An exact chiral amorphous spin liquid, *Nature Communications* **14**, 6663 (2023).
- [77] A. G. Grushin and C. Repellin, Amorphous and polycrystalline routes toward a chiral spin liquid, *Phys. Rev. Lett.* **130**, 186702 (2023).
- [78] S. Dusuel, K. P. Schmidt, J. Vidal, and R. L. Zaffino, Perturbative study of the kitaev model with spontaneous time-reversal symmetry breaking, *Phys. Rev. B* **78**, 125102 (2008).
- [79] H. Yao and S. A. Kivelson, Exact chiral spin liquid with non-abelian anyons, *Phys. Rev. Lett.* **99**, 247203 (2007).
- [80] K. Ray, S. Ananthavel, D. Waldeck, and R. Naaman, Asymmetric scattering of polarized electrons by organized organic films of chiral molecules, *Science* **283**, 814 (1999).
- [81] Q. Qian, H. Ren, J. Zhou, Z. Wan, J. Zhou, X. Yan, J. Cai, P. Wang, B. Li, Z. Sofer, *et al.*, Chiral molecular intercalation superlattices, *Nature* **606**, 902 (2022).
- [82] Z. Wan, G. Qiu, H. Ren, Q. Qian, D. Xu, J. Zhou, J. Zhou, B. Zhou, L. Wang, Y. Huang, *et al.*, Signatures of chiral superconductivity in chiral molecule intercalated tantalum disulfide (2023), Preprint, <http://arxiv.org/2302.05078>.
- [83] L. A. Wray, S.-Y. Xu, Y. Xia, D. Hsieh, A. V. Fedorov, Y. S. Hor, R. J. Cava, A. Bansil, H. Lin, and M. Z. Hasan, A topological insulator surface under strong coulomb, magnetic and disorder perturbations, *Nature Physics* **7**, 32–37 (2010).
- [84] F. Katmis, V. Lauter, F. S. Nogueira, B. A. Assaf, M. E. Jamer, P. Wei, B. Satpati, J. W. Freeland, I. Eremin, D. Heiman, *et al.*, A high-temperature ferromagnetic topological insulating phase by proximity coupling, *Nature* **533**, 513 (2016).
- [85] B. Sbierski, E. J. Dresselhaus, J. E. Moore, and I. A. Gruzberg, Criticality of two-dimensional disordered dirac

- fermions in the unitary class and universality of the integer quantum hall transition, *Phys. Rev. Lett.* **126**, 076801 (2021).
- [86] R. Resta, The insulating state of matter: a geometrical theory, *The European Physical Journal B* **79**, 121–137 (2011).
- [87] I. Souza, T. Wilkens, and R. M. Martin, Polarization and localization in insulators: Generating function approach, *Phys. Rev. B* **62**, 1666 (2000).
- [88] N. Marzari and D. Vanderbilt, Maximally localized generalized wannier functions for composite energy bands, *Phys. Rev. B* **56**, 12847 (1997).

## Supplemental material to the manuscript

In this supplemental material we provide technical details on the main paper, namely the T-matrix expansion of the self-energy I, the defect Hamiltonian II, the existence of a gap at arbitrarily small impurity densities III, the evaluation of the phase diagram IV, the verification of the thermal metal transition using CPGF methodsV and the existence of a spectral gap around the tri-critical point VI.

### I. T-MATRIX OF THE IMPURITY

We now explain how to get to the self-energy results quoted in the main paper. Consider the impurity  $V = V_{\square}$  of the main paper, depicted in Fig. 1. Choosing a basis consisting of the sites on one Honeycomb plaquette in clockwise fashion starting from  $r_0$  as indicated in the figure 1, the potential is represented by the matrix:

$$V = t_2 \begin{bmatrix} 0 & 0 & -i & 0 & i & 0 \\ 0 & 0 & 0 & -i & 0 & i \\ i & 0 & 0 & 0 & -i & 0 \\ 0 & i & 0 & 0 & 0 & -i \\ -i & 0 & i & 0 & 0 & 0 \\ 0 & -i & 0 & i & 0 & 0 \end{bmatrix} \quad (1)$$

The lattice Green's function at zero energy between these six sites on the Honeycomb is given by

$$g = \begin{bmatrix} 0 & \frac{1}{3} & 0 & -\frac{\sqrt{3}}{2\pi} & 0 & \frac{1}{3} \\ \frac{1}{3} & 0 & \frac{1}{3} & 0 & -\frac{\sqrt{3}}{2\pi} & 0 \\ 0 & \frac{1}{3} & 0 & \frac{1}{3} & 0 & -\frac{\sqrt{3}}{2\pi} \\ -\frac{\sqrt{3}}{2\pi} & 0 & \frac{1}{3} & 0 & \frac{1}{3} & 0 \\ 0 & -\frac{\sqrt{3}}{2\pi} & 0 & \frac{1}{3} & 0 & \frac{1}{3} \\ \frac{1}{3} & 0 & -\frac{\sqrt{3}}{2\pi} & 0 & \frac{1}{3} & 0 \end{bmatrix}, \quad (2)$$

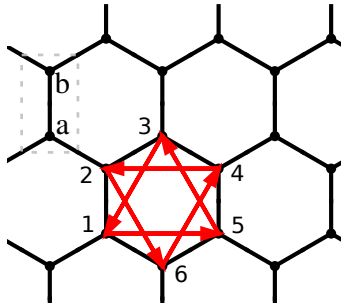


FIG. 1: The Honeycomb lattice and our choice for the an a,b sublattice. The red arrows indicate the orientation for a positive sign of the imaginary NNN hopping of the impurity. The site indices 1 through 6 shows the convention for the basis in which we represent the matrices of the impurity.

where we have used the *exact* value of the lattice Green's function connecting nearest-neighbours (NN) and next-NN sites [1]. Following Titov *et al* [1, 2] we decompose the lattice wave-function of the clean model  $\Psi(r)$  into the form

$$\Psi(r) = \sqrt{A} \left( e^{iK \cdot r} [\psi_{K_a}(r)\delta_{r_a} + \psi_{K_b}(r)\delta_{r_b}] + e^{iK' \cdot r} (\psi_{K'_a}(r)\delta_{r_a} + \psi_{K'_b}(r)\delta_{r_b}) \right), \quad (3)$$

where  $A$  is the area of the unit cell  $\delta_{r_\alpha}$  is an indicator function for the sublattice  $\alpha$  and  $K, K'$  represents the two inequivalent Dirac valley momenta. The envelope wave-function  $|\psi\rangle = (\psi_{K_a}, \psi_{K_b}, \psi_{K'_a}, \psi_{K'_b})$  obeys the Dirac equation

$$\frac{3t}{2} (\partial_x \sigma_x \tau_z + \partial_y \sigma_y) |\psi\rangle = E |\psi\rangle \quad (4)$$

where  $\sigma$  acts on the sublattice d.o.f and  $\tau$  on the valley d.o.f. The Dirac wavefunction can be related to the lattice wave function using the vectors

$$\langle u_a | = (e^{iK \cdot r}, 0, e^{iK' \cdot r}, 0) \quad \langle u_b | = (0, e^{iK \cdot r}, 0, e^{iK' \cdot r}) \quad (5)$$

such that  $\Psi(r) = A\delta_{r_\alpha} \langle u_\alpha | \psi \rangle$ . We construct the matrix  $X$  whose rows consist of the vectors  $|u\rangle$  evaluated on the sites of the chosen basis with  $r_0 = 0$ :

$$X = \sqrt{A} \begin{bmatrix} 1 & 0 & 1 & 0 \\ 0 & -1 & 0 & -1 \\ e^{-\frac{2i\pi}{3}} & 0 & e^{\frac{2i\pi}{3}} & 0 \\ 0 & e^{-\frac{i\pi}{3}} & 0 & e^{\frac{i\pi}{3}} \\ e^{\frac{2i\pi}{3}} & 0 & e^{-\frac{2i\pi}{3}} & 0 \\ 0 & e^{\frac{i\pi}{3}} & 0 & e^{-\frac{i\pi}{3}} \end{bmatrix} \quad (6)$$

Using  $X$  we can obtain the impurity in the Dirac-fermion language. Indeed,

$$X^\dagger V X = A3\sqrt{3}t_2\sigma_z\tau_z \quad (7)$$

which is also the result we obtain by Fourier transforming the impurity potential and expanding around the Dirac points to lowest order. The effective impurity potential is renormalized by multiple scattering events and given by the T-matrix:

$$\tilde{T} = (1 - Vg)^{-1}V \quad (8)$$

We observe that the T-matrix has poles at  $t_2 \approx \pm 0.948$  which correspond to zero energy bound states also found from exact diagonalization of the full Hamiltonian. The eigenspace corresponding to the pole has dimension two. As emphasized by Titov *et al*, the T-matrix can depend on  $r_0$ . Indeed, in general we must write

$$X(r_0) = XW(r_0), \quad W = \begin{bmatrix} e^{iK \cdot r_0} & 0 & 0 & 0 \\ 0 & e^{iK \cdot r_0} & 0 & 0 \\ 0 & 0 & e^{-iK \cdot r_0} & 0 \\ 0 & 0 & 0 & e^{-iK \cdot r_0} \end{bmatrix} \quad (9)$$

In the Dirac basis the T-matrix is then of the form

$$T = X^\dagger \tilde{T} X = T_{\mathbf{R}}(0) = \frac{A3\sqrt{3}t_2}{t_2^2/t_c^2 - 1} [\sigma_z\tau_z - \frac{t_2}{t_c}\sigma_x(\tau_x \cos f_{\mathbf{R}} + \tau_y \sin f_{\mathbf{R}})], \quad t_c = \frac{2\sqrt{3}\pi}{3\sqrt{3} + 2\pi}t$$

The anti-diagonal elements of  $T(r_0)$  acquire a phase factor leading to the oscillations with  $f_{\mathbf{R}} = 2K \cdot \mathbf{R}$  which correspond to the third roots of unity. Therefore T-matrix averaged over impurity positions is diagonal and the self-energy in the T-matrix approximation is:

$$\Sigma = \frac{\rho}{A} \langle T(r_0) \rangle = \frac{3\sqrt{3}\rho t_2}{t_2^2/t_c^2 - 1} \sigma_z\tau_z \quad (10)$$

We now consider the self-energy at  $E \neq 0$ . The T-matrix at  $E$  can be obtained via [3]:

$$T(E) = \frac{T(0)}{1 - T(0)\gamma(E)}, \quad \gamma = \lim_{r \rightarrow 0} G_0(E, r) - G_0(0, r) \approx \frac{1}{2\pi v^2} E \log iE \quad (11)$$

More specifically, we compute

$$\Sigma(E; t_2) = \frac{\rho}{A(1 - 2\beta^2(1 + t_2^2)\gamma^2 + [\beta^2(t_2^2 - 1)\gamma^2]^2)} (\gamma[\beta^2(1 + t_2^2) + (\beta^2(t_2^2 - 1)\gamma)^2]\sigma_0\tau_0 + \beta [1 + (\beta^2(t_2^2 - 1)\gamma)^2]\sigma_z\tau_z) \quad (12)$$

with  $\beta = \frac{A3\sqrt{3}t_2}{t_2^2/t_2^2 - 1}$ . The spectral function is evaluated using

$$\mathbf{A}(E, k) = -\frac{1}{\pi} \Im \text{Tr} G(E - i\delta, k) = \Im \frac{4}{\pi} \left( \frac{E - \Sigma_{00}}{(E - \Sigma_{00})^2 - \Sigma_{zz}^2 - v^2 k^2} \right) \quad (13)$$

Integrating over momentum we get the density of states DoS:

$$N(E) = \frac{E - \Sigma_{00}}{4\pi v^2} \log((E - \Sigma_{00})^2 - \Sigma_{zz}^2) \quad (14)$$

## II. DEFECT HAMILTONIAN

While the previous technique gave us the exact self-energy at the  $K$  points it is worthwhile to understand also the bare impurity potential at first order in momentum for the purpose of gaining an intuition of the scattering processes involved in the sign reversal of the mass, and an analysis of the topology of the defect Hamiltonian.

For the following discussion we take  $t = a = 1$ . Expanding the impurity potential into momentum space we obtain:

$$V = it_2 \sum_{p,q} e^{i(k-q)\cdot R_0} ((e^{ip\cdot a_1} + e^{-iq\cdot(a_1-a_2)} + e^{i(p\cdot(a_1-a_2)-q\cdot a_1)})c_p^{A\dagger}c_q^A) \quad (15)$$

$$+ (e^{iq\cdot a_2} + e^{ip\cdot(a_1-a_2)} + e^{-i(p\cdot a_2+q\cdot(a_1-a_2))})c_p^{B\dagger}c_q^B + h.c. \quad (16)$$

where  $a_i$  are the lattice vectors and  $A|B$  index the sublattice. Now split the sum into  $\sum_p = \sum_k \sum_{k'}^{K}$  and introduce the operator  $\psi_{KR_0A}(k) = e^{-iK\cdot R_0}c_{K+k}^A$  such that e.g.  $\sum_k k_x e^{-iK\cdot R_0}\psi_{KR_0A}(k) = e^{-iK\cdot R_0}i\partial_x\psi_{Ka}(R_0)$  and similarly for the B sublattice, but keeping in mind that we placed the origin at the A site. We obtain:

$$V_{R_0} = \int dr \delta(r - R_0) \frac{3t_2}{2} \bar{\psi}(r) (-i\tau_x(r)\sigma_z\partial_x + i\tau_y(r)\partial_y + 2\sqrt{3}\sigma_z\tau_z)\psi(r) \quad (17)$$

where  $\tau_{x|y}(R_0) = U_{R_0}\tau_{x|y}^f U_{R_0}^\dagger$  with  $\tau^f$  a fixed choice of basis for the Pauli matrices and  $U(R_0) = \exp \frac{i}{2}(K - K') \cdot R_0\tau_z$ . To analyze the topology of the defect Hamiltonian we also add the additional term generated at the level of the T-matrix and change notation by using the  $\gamma$  matrices which form a four-dimensional representation of the Clifford algebra, we obtain:

$$h = \frac{3}{2}\gamma_1(1 + t_2 i\delta_{R_0}\tilde{\gamma}_4(r)\gamma_5)\partial_x + \frac{3}{2}\gamma_2(1 + t_2 i\delta_{R_0}\tilde{\gamma}_4(r)\gamma_5)\partial_y + \delta_{R_0}(im(t_2)\gamma_1\gamma_2 + M(t_2)\tilde{\gamma}_3(r)) \quad (18)$$

where  $\tilde{\gamma}_{3|4}(r) = e^{(K-K')\cdot\frac{\sigma}{2}\gamma_3\gamma_4}\gamma_{3|4}e^{-(K-K')\cdot\frac{\sigma}{2}\gamma_3\gamma_4}$ ,  $m$  is the topological mass and  $M$  the valley mixing mass. According to the topological defect classification of Theo and Kane the defect may be topological, i.e. realize a vortex defect, if the mass term  $M\tilde{\gamma}_3(r)$  has an odd winding number and the clean system has an odd Chern number. However,  $M\tilde{\gamma}_3(r)$  does not wind and furthermore the zero mode is associated to a gap closing of the defect Hamiltonian, i.e.  $M = m$ , and hence falls outside the aforementioned classification scheme.

## III. EXISTENCE OF A GAP FOR ARBITRARILY SMALL DENSITIES

Given that the mass terms are added only in a local fashion, the appearance of global spectral gap at infinitesimally small impurity densities might seem surprising. However, in light of the fact that corrections to the unperturbed Green's function coming from an individual impurity at, e.g., the origin arise as

$$G(r, r, E) = G_0(r, r, E) + \sum_{r_1, r_2} G(r, r_1, E) T \delta(0, r_1) \delta(r_2, 0) G(r_2, r, E) \quad (19)$$

$$= G_0(r, r, E) + T G_0(r, 0, E) G(0, r, E), \quad (20)$$

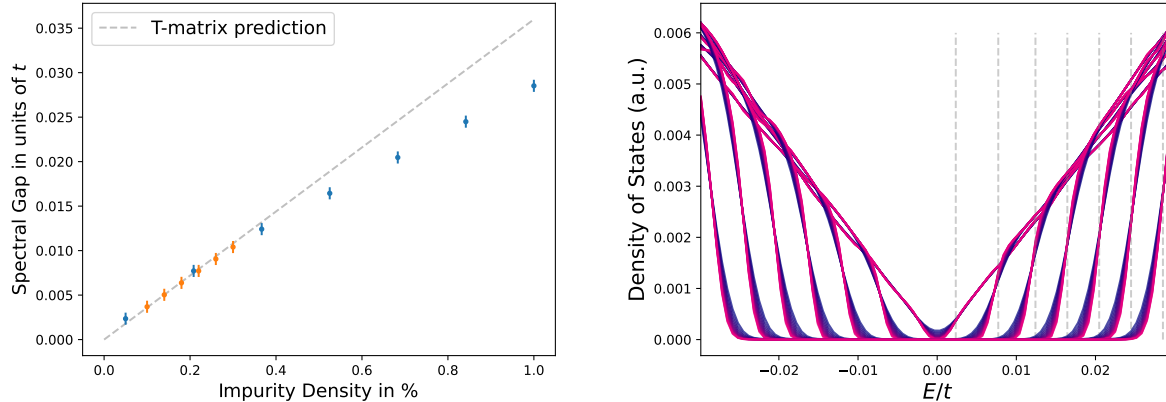


FIG. 2: The spectral gap calculated from the DoS via the CPGF method for various densities at fixed  $t_2 = 0.5t$  (left). The yellow points are calculated with  $1.4e9$  sites and  $1.6e4$  moments, the blue points with  $0.6e9$  sites and  $1.2e4$  moments (blue). The spectral gap is calculated by computing the maximum of  $\frac{d}{dE}[\rho_{N_{max}}(E) - N_{n_{min}}(E)]$  where  $N_n$  is the density of states calculated at  $n$  moments. Note that the T-matrix prediction contains no free parameter. In the right panel we show full density of states as a corresponding to the blue data points in the left panel for various moments from small (dark blue) to large (magenta). The vertical dashed lines indicate the estimated value of the spectral gap in the thermodynamic limit.

where we have assumed an on-site impurity and separated the spatial dependence of the  $T$ -matrix into the delta functions, the result is actually quite natural. Indeed, the local Greens function at any point will receive contributions from all impurities which, at low energies, go as the square of the inverse of the distance, therefore establishing a global gap. For instance, consider the worst case scenario, namely for the chosen point  $r$  all impurities have the maximal distance  $D$  to  $r$ . Assuming that the impurities are distributed isotropically, we can think of them as modeled by a uniform density on a ring  $\nu(r) = \frac{\rho}{2}|r|\delta(|r| - D)$ , where the factor of  $|r|$  comes from the requirement that the impurity density with respect to the area enclosed by the circle is kept constant. Performing the integral

$$\sum_{R_i} T G_0(r, R_i, E) G_0(R_i, r, E) \propto T \int \int \nu(r) \frac{1}{|r|^2} |r| d|r| d\phi = \pi \rho T \quad (21)$$

we conclude that the correction does not depend on  $D$  and is larger than zero. We can see that the T-matrix prediction for the global spectral gap also holds up well for the CPGF data in fig. 2 at small densities. Note that for densities larger than 0.005 higher order effects become noticeable.

#### IV. PHASE DIAGRAM FROM SMALL SUPERCCELL

We now explain the method we used to determine the phase diagram of our model. Using the operators

$$V_j = P \exp\left(i \frac{2\pi}{L_j} x_j\right) P + Q, \quad Q = 1 - P \quad (22)$$

where  $P$  is the Fermi-projector,  $x_j$  is the position operator in direction  $j$  and  $L$  the length of the system, the Bott index defined as

$$\text{Bott}(P) = \text{Re} \frac{1}{2\pi i} \text{Tr} \log(V_{x_1} V_{x_2} V_{x_1}^\dagger V_{x_2}^\dagger), \quad (23)$$

corresponds to the Chern number [4]. The ground state manifold over the twist-angle parameter space also contains information on localization. Indeed, the localization tensor  $\lambda$  is proportional to the quantum metric and the gauge invariant part of the Wannier-Spread-Functional and computed by [5, 6]:

$$\lambda_{11} := \frac{\Re}{2\pi} \log \det V_1 V_1^\dagger \propto \int_0^\infty \Re \frac{\sigma_{11}(\omega)}{\omega} d\omega, \quad (24)$$

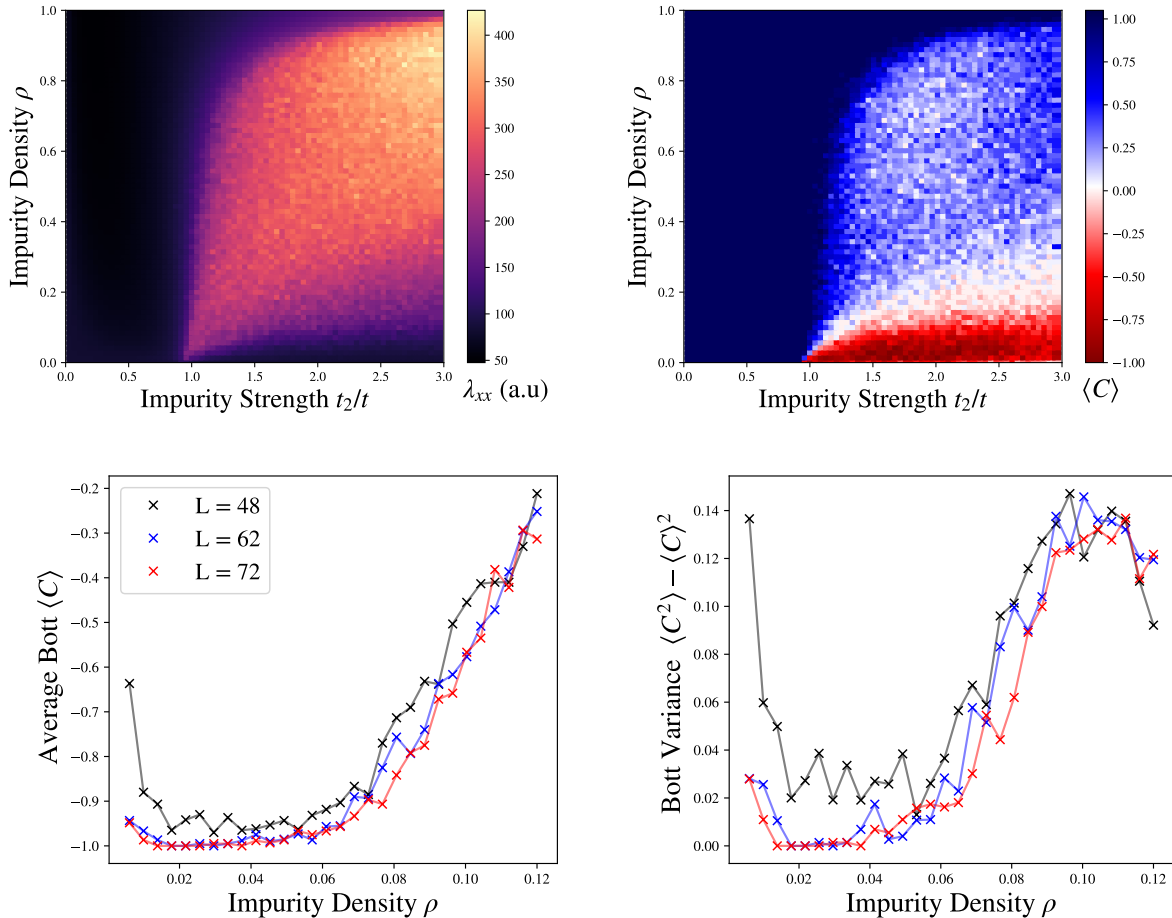


FIG. 3: The localization length  $\lambda_{xx}$  (top left) and the average Bott index (top right) in the parameter space spanned by the impurity density and strength. Variance (bottom left) and average (bottom right) of the Bott index at  $t_2 = 2t$  as a function of impurity density  $\rho$  evaluated for system sizes  $L = 42, 62, 72$  each data point has been averaged over 175 samples.

where  $\sigma$  is the conductivity tensor. From the second equality [6] it is clear that a divergent  $\lambda$  is a marker for delocalization. Note that in finite systems the divergence caused by a finite dc conductivity is cut off. Figure 3 shows the value of these quantities in the parameter space spanned by impurity strength and density calculated over 40 disorder realizations and for  $1.44 \times 10^3$  sites.

The small size of the  $C = -1$  gap makes the evaluation of the Chern number especially susceptible to fluctuations caused by finite size effects. By increasing the system size for a select value of  $t_2 = 2J$  we confirm that these fluctuations can be vanquished by increasing the system size, and  $\langle C \rangle$  stays below 0.9 up to densities of 0.08.

The phase boundaries and their error shown in Fig. 1 of the main paper were calculated from the Bott index data by fitting the edges extracted from the shape satisfying  $\langle C \rangle > a$ , where  $a = 0.5 \pm 0.25$  for the  $C = 1$  phase and  $a = -0.5 \pm 0.25$  for the  $C = -1$  phase.

## V. TRANSITION TO THERMAL METAL

The thermal metal is characterized by a logarithmic divergence of the density of states and the conductivity [7]. Meanwhile an insulator has a vanishing dc longitudinal conductivity and usually a vanishing or finite density of states. However, Griffiths effects (rare region effects) can cause a power law diverging density of states even in the insulating phase [8]. We use the logarithmic divergences to confirm the existence of a thermal metal phase suggested by the small super-cell calculations.

Note that when it comes to the properties of the system at energies smaller than the CPGF resolution  $\eta$  the logarithmic

mic divergence effects are cut off and e.g. the DoS approaches a constant. The value of this constant however depends on  $\eta$  in the same way as the density of states depends on the energy [9]. In fact we can also associate an effective length scale  $L^*$  to  $\eta$  [10], namely  $L^*$  is the length of the clean model with finite size level spacing  $\eta$  at the Dirac point:  $L^* = \frac{\pi v}{\eta}$  such that  $\eta^{-1}$  is a natural scaling variable. This is also justified by a different line of arguments discussed by Wang *et. al.* [9]. For conductivity calculations  $\eta$  refers to the resolution of the rescaled Hamiltonian and enters as a fixed parameter in the CPGF because it is computed with a Lorentz-Kernel [11]. For the calculation of the DoS  $\eta$  is given in arbitrary units (a.u.) because we use the Jackson-kernel [11] where only the number of moments are fixed and the proportionality constant to the resolution is not known. However, these details don't matter to the scaling arguments we present.

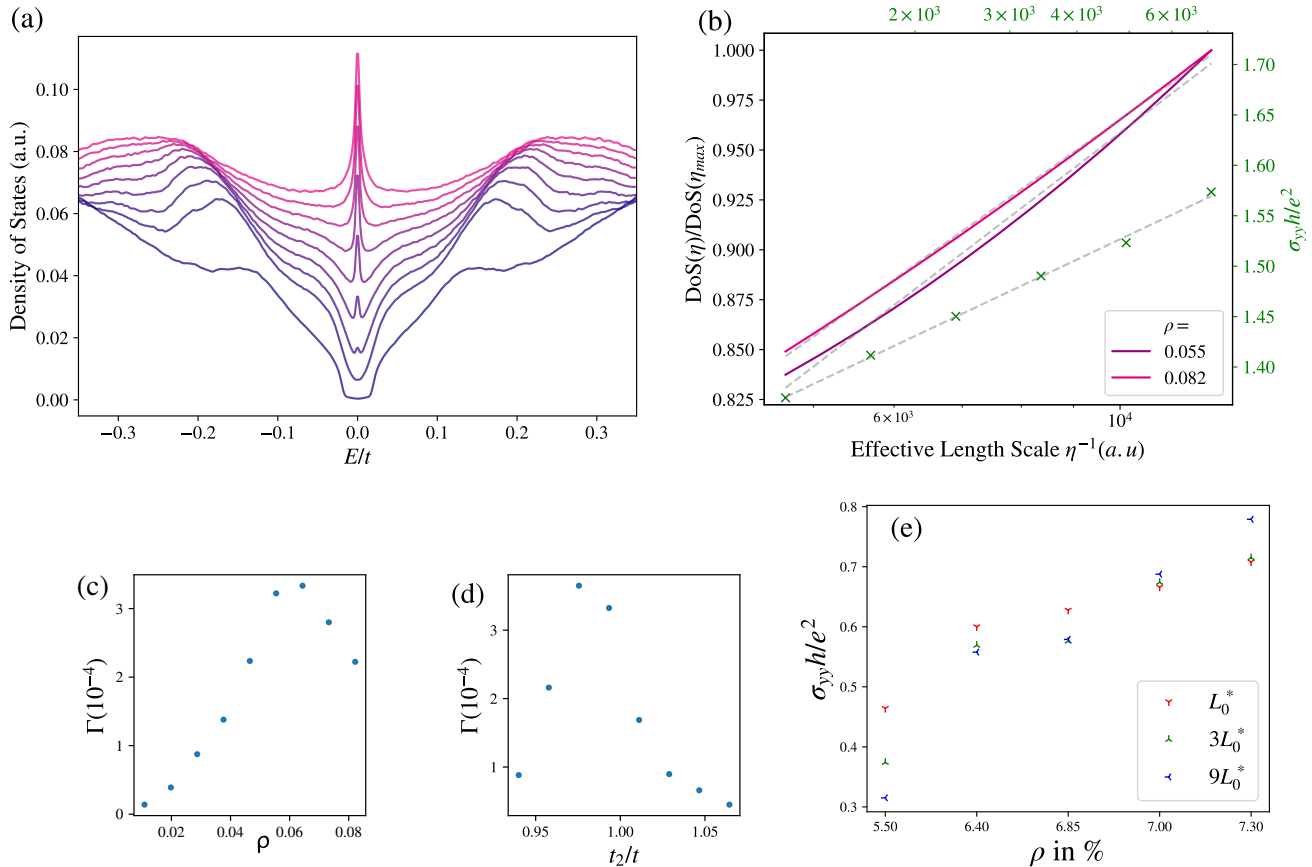


FIG. 4: (a) The evolution of the DoS ( $N = 2.95 \times 10^8$  and 10240 moments) calculated at  $t_2 = 1.1$  for various densities  $\rho$ . The color helps to distinguish the different values of  $\rho$  from  $\rho = 0.002$  blue to  $\rho = 0.1$  magenta. The DoS is an increasing function of  $\rho$  for the shown parameters. (b) The divergence of the density of states, rescaled to a maximum of one for better visibility of non-linear features. The green dots represent the conductivity as a function of the effective length scale  $\eta^{-1}$ . The dashed lines represent a logarithmic fit to the CPGF data. (c) / (d) the error of the fits to the DoS as a function of  $\rho$  (c) /  $t_2$  (d). (e) Longitudinal conductivity at fixed  $t_2 = 1.1t$  and varying  $\rho$  ( $N = 2.15 \times 10^9$ ,  $L_0$  corresponds to  $\eta = 0.008$ ).

In Fig. 4 (a) we show the evolution of the DOS at  $t_2 = 1.5t$  in the interval between  $\rho = 0.002, 0.1$ . The data is calculated for  $5.8 \times 10^8$  sites and  $1.23 \times 10^4$  moments. We observe that there are three regimes; a Chern insulator with a spectral gap, a Chern insulator with a diverging DoS and a thermal metal with a logarithmically diverging DoS. The transition between the Griffiths phase and the thermal metal can roughly be estimated by a maximum in the error  $\Gamma$  of a linear fit to  $\text{DoS}(z = \log(\eta^{-1}))$ . For example at  $t_2 = 1.5t$  we find that there is a maximum at about  $\rho = 0.65 \pm 0.05$ , and a similar behaviour appears when keeping the density fixed at  $\rho = 0.1$  and varying  $t_2$ . The increase of  $\Gamma$  may be explained by assuming a weak non-universal power law divergence whose exponent increases towards the critical density. The lack of a discontinuous jump when reaching the thermal metal side may be attributed to the fact that we probe the scaling at values of  $\eta$  where signs of the fixed point representing the transition remain. In 4 (b) we show

the divergence of the DoS in the Griffiths phase, as well as the scaling of the DoS and conductivity in the thermal metal, which we find well approximated as logarithmically divergent. The longitudinal dc conductivity is calculated for systems with  $2.15 \times 10^9$  sites and we find that a moment cut off of  $\frac{1.4}{\eta}$  converges the data to three significant digits. At  $\rho = 0.064$  the conductivity decreases with the effective length scale, while for  $\rho = 0.0700$  it is increasing. At a value of  $\rho = 0.685$  we observe that a decrease of the conductivity from  $L_0^*$  to  $3L_0^*$ , while for an increase from  $3L_0^*$  to  $9L_0^*$  the conductivity does not decrease. Considering that the TM-CI transition is expected to have a scale invariant conductivity, this suggests that the value of  $\rho = 0.685$  is very close to critical which is consistent with the phase boundary calculated via the small super-cell approach predicting the transition to be at  $\rho = 0.070 \pm 0.02$ . Note that because the focus of this work is not an analysis of the criticality of the Anderson transitions, we are content with establishing the existence of the phases and do not attempt a precise evaluation of the critical parameters, which could be efficiently done by e.g the  $\Gamma$  scaling method. Although we remark that the prediction for the position of the tri-critical point is *exact*.

To explain how same sign mass disorder can give rise to a thermal metal phase consider that in the limit of large  $t_2$  our model approaches the problem of random sign  $\frac{\pi}{2}$  fluxes on a triangular lattice which maps to the random sign Majorana problem studied in the context of topological liquid nucleation [12, 13]. Here the probability of a sign flip resembles the density  $\rho$  in our model. For  $\rho$  close to 1 the analogy is clear considering that there are  $1 - \rho$  vacancies which create a plaquette with a flipped flux. Meanwhile, for small  $\rho$  events where triangles bunch together can prevent the scattering process that leads to a sign inversion and so increasing the density  $\rho$ , and therefore the probability of such events, increases the effective sign disorder. The phase diagram of the random sign Majorana problem is equivalent to ours at a cut of constant  $t_2 > t_2^c$ . In particular it contains no trivial insulating phase. Introducing a mass term by a sublattice-staggered potential would introduce a trivial insulating phase and split the tri-critical point into two tri-critical points pushed to a finite density.

## VI. GAP AROUND THE TRI-CRITICAL POINT

The spectral function data in Fig. 2 a) of the main paper was calculated for  $N = 2.95 \times 10^8$  and 4608 moments. Meanwhile the parameters for the DoS data were  $N = 2.95 \times 10^8$  and 10240 moments.

In Fig. 5 we plot the DoS at the neutrality point for  $\rho = 0.0015$  as a function of the resolution  $\eta$  for various values of  $t_2$ . We observe that away from the critical  $t_2$  the DoS starts to decrease with the resolution  $\eta$ . The closer we are to the transition, the smaller the value of  $\eta$  where this behaviour sets in. In our case we conclude that the  $t_2$  with a metallic phase are a subset of the interval between  $t_2 = 0.949t$  and  $t_2 = 0.951t$ . Deviation from the T-matrix prediction  $t_c \approx 0.948t$  is to be expected given that including a self-consistency condition can change the value of  $t_c$ . Indeed we observe numerically that  $t_c$  is an increasing function of  $\rho$ .

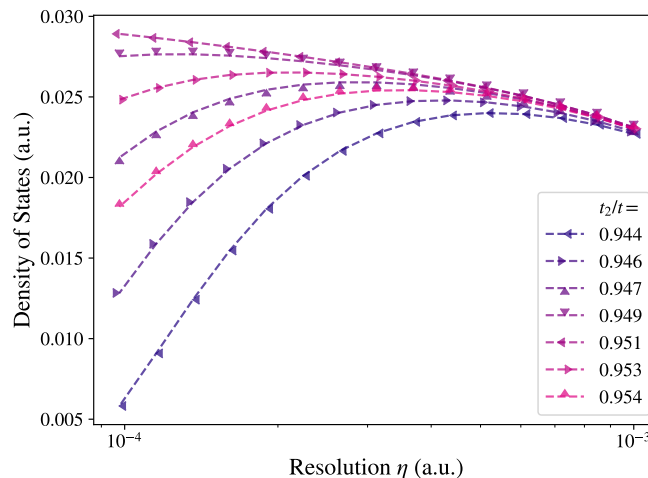


FIG. 5: The DoS at  $E = 0$  as a function of the energy resolution  $\eta$  for  $\rho = 0.0015$  and various  $t_2$  around the critical value  $t_2^c = 0.950 \pm 0.01$ .

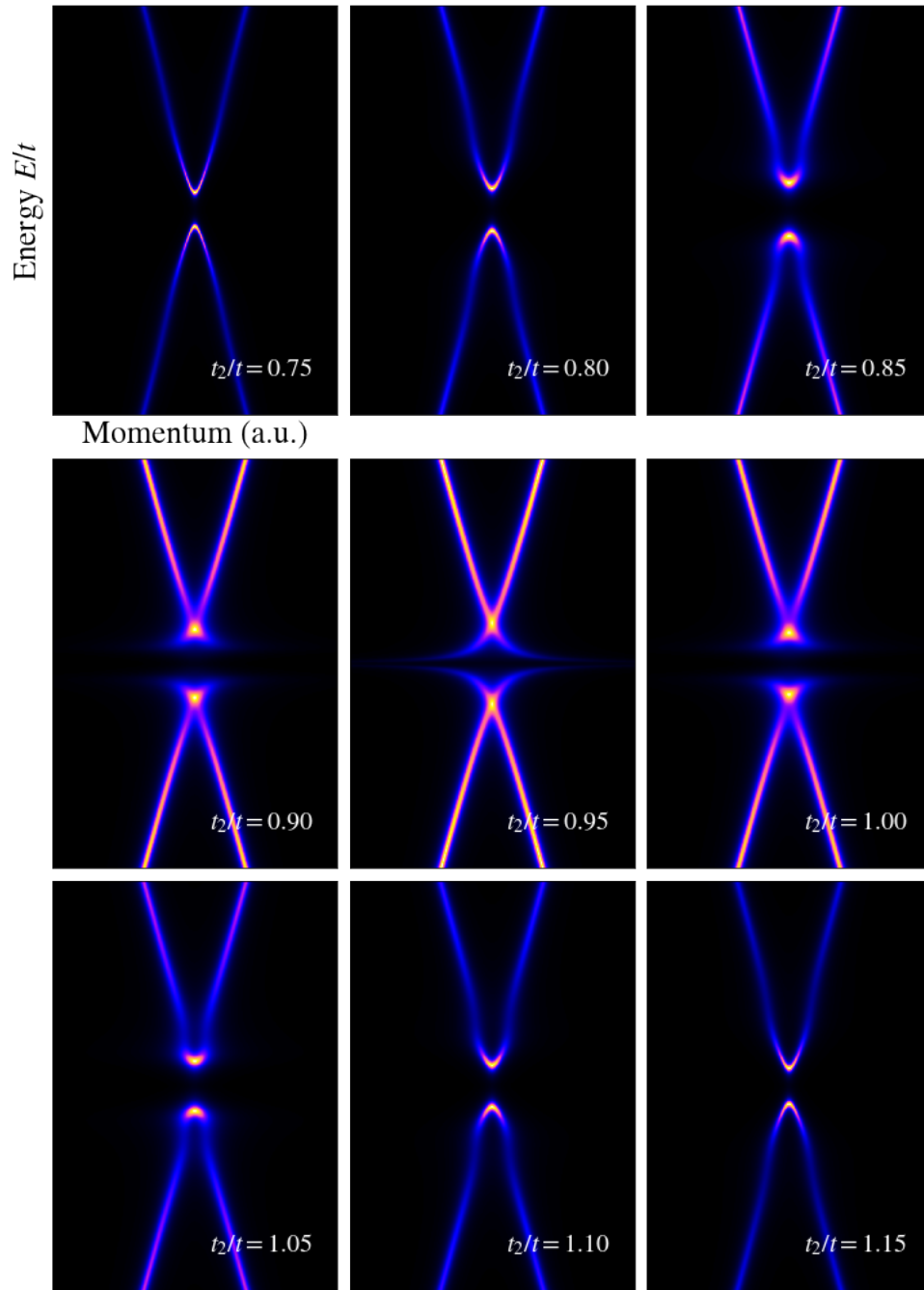


FIG. 6: Evolution of the spectral function as a function of  $t_2$  calculated with the T-matrix approximation to the self-energy at  $\rho = 0.0015$

- 
- [1] J. Schelter, P. M. Ostrovsky, I. V. Gornyi, B. Trauzettel, and M. Titov, Color-dependent conductance of graphene with adatoms, *Phys. Rev. Lett.* **106**, 166806 (2011).
  - [2] P. M. Ostrovsky, M. Titov, S. Bera, I. V. Gornyi, and A. D. Mirlin, Diffusion and criticality in undoped graphene with resonant scatterers, *Phys. Rev. Lett.* **105**, 266803 (2010).
  - [3] P. Kot, J. Parnell, S. Habibian, C. Stra er, P. M. Ostrovsky, and C. R. Ast, Band dispersion of graphene with structural defects, *Phys. Rev. B* **101**, 235116 (2020).
  - [4] M. B. Hastings and T. A. Loring, Topological Insulators and  $C^*$ -Algebras: Theory and Numerical Practice, *Annals of Physics* **326**, 1699 (2010), arXiv:1012.1019.
  - [5] R. Resta, The insulating state of matter: a geometrical theory, *The European Physical Journal B* **79**, 121–137 (2011).
  - [6] I. Souza, T. Wilkens, and R. M. Martin, Polarization and localization in insulators: Generating function approach, *Phys. Rev. B* **62**, 1666 (2000).
  - [7] F. Evers and A. D. Mirlin, Anderson transitions, *Rev. Mod. Phys.* **80**, 1355 (2008).
  - [8] A. Mildenberger, F. Evers, R. Narayanan, A. D. Mirlin, and K. Damle, Griffiths phase in the thermal quantum hall effect, *Phys. Rev. B* **73**, 121301 (2006).
  - [9] T. Wang, Z. Pan, T. Ohtsuki, I. A. Gruzberg, and R. Shindou, Multicriticality of two-dimensional class-d disordered topological superconductors, *Phys. Rev. B* **104**, 184201 (2021).
  - [10] A. Ferreira and E. R. Mucciolo, Critical delocalization of chiral zero energy modes in graphene, *Phys. Rev. Lett.* **115**, 106601 (2015).
  - [11] A. Wei e, G. Wellein, A. Alvermann, and H. Fehske, The kernel polynomial method, *Reviews of Modern Physics* **78**, 275–306 (2006).
  - [12] C. R. Laumann, A. W. Ludwig, D. A. Huse, and S. Trebst, Disorder-induced majorana metal in interacting non-abelian anyon systems, *Physical Review B - Condensed Matter and Materials Physics* **85**, 161301 (2012).
  - [13] E. Grosfeld and A. Stern, Electronic transport in an array of quasiparticles in the non-abelian quantum hall state, *Phys. Rev. B* **73**, 201303 (2006).